ACES Asian Chemical Editorial Society

DOI: 10.1002/cnma.202000541

CHEMNANOMAT
Full Paper

Cesium Ion-Mediated Microporous Carbon for CO_2 Capture and Lithium-Ion Storage

Hyeon Jeong Lee,[a] Dongah Ko,[b] Joo-Seong Kim,[b] Youngbin Park,[a] Insu Hwang,[a] Cafer T. Yavuz,[b, c] and Jang Wook Choi*[a, d]

Abstract: Activated carbon has been used in a wide range of applications owing to its large specific area, facile synthesis, and low cost. The synthesis of activated carbon mostly relies on potassium hydroxide (KOH)-mediated activation which leads to the formation of micropores (< 2 nm) after a washing step with acid. Here we report the preparation of activated carbon with an anomalously large surface area (3288 $m^2 g^{-1}$), obtained by employing an activation process mediated by cesium (Cs) ions. The high affinity of the carbon lattice for Cs ions induces immense interlayer expansion upon complexation of the intercalant Cs ion with the carbon host. Furthermore, the Cs-activation process maintains the nitrogen content of the carbon source by enabling the activation process at low temperature. The large surface area and well-preserved nitrogen content of Cs-activated carbon takes advantage of its enhanced interaction with CO_2 molecules (for superior CO_2 capture) and lithium ions (for improved Li ion storage), respectively. The present investigation unveils a new approach toward tuning the key structural properties of activated carbon; that is, controlling the affinity of the carbon host for the intercalant ion when they engage in complex formation during the activation process.

Introduction

Activated carbon materials have been widely used as dry sorbents for gas capture as well as active materials for electrochemical energy storage.[1–3] Both of these applications of activated carbon rely on the adsorption of carrier ions or gas molecules onto its surface such that the storage capacity is by and large proportional to the surface area of activated carbon.[4–7] In this respect, potassium hydroxide (KOH)-mediated chemistry[8,9] is the most widely adopted activation method to obtain carbon materials with micropores (< 2 nm in diameter) based on the following reaction:[1,10–14] 6 $KOH(s) + C(s) \rightarrow 2\ K(s) + 3\ H_2(g) + K_2CO_3(s)$. At a sufficiently high temperature such as 600 °C, the K_2CO_3 product is decomposed into K_2O and CO_2, and K_2O is further decomposed into metallic K and CO at higher temperatures over 700 °C.[1,10,11,15] Even at a low temperature below 600 °C, KOH is dehydrated to K_2O, which reacts with carbon to form K_2CO_3. Micropores are finally formed in the original carbon powder by gasification of the carbon substrate and as a result of removing the solid intermediates and final products (K_2CO_3, K_2O, and K) by washing with acid. Hence, to allow the reaction to fully proceed to metallic K in high yield, KOH activation requires a high temperature (i.e., 700 °C).[1,10] However, the activation of KOH at such a high temperature tends to eliminate the hetero-atoms that are intrinsically present in the original carbon material, which are often useful for increasing the amount of carrier ions or gas molecules taken up by enhanced molecular interaction involving lone-pair electrons.[16–19] Therefore, other chemistries based on low-temperature activation would be worth exploring to achieve both a large surface area and hetero-atom content simultaneously, although these two parameters are often mutually exclusive when activated carbon is synthesized.

In this research, we report a low-temperature activation process that engages cesium (Cs) ions, instead of K ions, to catch the aforementioned two rabbits (large surface area and hetero-atom content) at the same time and use the resulting activated carbon for CO_2 capture and Li ion storage. To evaluate the viability of retaining the nitrogen (N) content of the final compound, a natural carbon source by name of *Spongia officinalis*, a hermaphroditic animal, was chosen as precursor material. Even though CsOH activation shares the reaction pathway of its KOH counterpart, Cs-activation requires a much lower temperature of 400 °C because the formation energy of Cs-sp^2 carbonaceous material is far lower than that of its K-equivalent; furthermore, penetration of the carbon framework by Cs ions toward the activation of the corresponding carbonaceous material is preferable.[20,21] As a result of the facile Cs ion-mediated activation, microporous carbon with a specific surface area of 3288 $m^2 g^{-1}$ and decent nitrogen content was obtained. By taking advantage of these key features, this microporous

[a] Dr. H. J. Lee, Y. Park, I. Hwang, Prof. J. W. Choi
School of Chemical and Biological Engineering and Institute of Chemical Processes
Seoul National University
1 Gwanak-ro, Gwanak-gu, Seoul 08826 (Republic of Korea)
E-mail: jangwookchoi@snu.ac.kr

[b] Dr. D. Ko, Dr. J.-S. Kim, Prof. C. T. Yavuz
Graduate School of Energy, Environment, Water, and Sustainability (EEWS)
Korea Advanced Institute of Science and Technology (KAIST)
291 Daehak-ro, Yuseong-gu, Daejeon 34141 (Republic of Korea)

[c] Prof. C. T. Yavuz
Department of Chemical and Biomolecular Engineering
Korea Advanced Institute of Science and Technology (KAIST)
291 Daehak-ro, Yuseong-gu, Daejeon 34141 (Republic of Korea)

[d] Prof. J. W. Choi
Department of Materials Science and Engineering
Seoul National University
1 Gwanak-ro, Gwanak-gu, Seoul 08826 (Republic of Korea)

Supporting information for this article is available on the WWW under https://doi.org/10.1002/cnma.202000541

carbon exhibited unusually high CO_2 uptake of 483 mg g^{-1} at 273 K and a high specific capacity of 115 mAh g^{-1} for Li ion storage in Li ion capacitors. The present investigation opens a new avenue toward upgrading the key properties of long-standing and widely used activated carbon by introducing distinct ion-to-carbon interaction.

Results and Discussion

Cs-activated carbon was synthesized by following the classical chemical activation method but using CsOH as the activation agent instead. A typical KOH-based chemical activation procedure[8,22,23] was also employed for comparison purposes. Marine sponge pre-carbonized at 300 °C was mixed with KOH or CsOH and activated at various temperatures. The resultant activated carbon materials are hereafter referred to as Cs-sponge and K-sponge, respectively. Detailed synthetic procedures are described in the Experimental Section. The drastic volume expansion resulting from Cs-activation is clearly observable on the digital photographs (Figure 1a). Even at the low temperature of 400 °C, the Cs-sponge underwent an unusually large volume expansion during activation. In sharp contrast, the K-sponge exhibited negligible volumetric expansion even after activation processes at temperatures as high as 600 °C. The morphologies of the K-sponge and Cs-sponge were visualized in comparison with that of the pre-carbonized sponge by scanning electron microscopy (SEM) (Figure 1b–d). The SEM image of the pre-carbonized sponge (denoted as *c*-sponge) indicates that pre-carbonization did not markedly change the original tubular morphology of the marine sponge. Similarly, KOH activation at 600 °C also largely retained the tubular morphology of the marine sponge although the tubes were ruptured at certain locations. Because the pore size was limited to below 2 nm, SEM analysis was not able to detect the pores at all, even after activation. Contrary to these two cases, in the case of CsOH activation at 600 °C, the tubular morphology of the *c*-sponge was entirely destroyed and transformed into a sheet-type one, thereby reflecting severe activation by the Cs ions.

The surface areas of the K-sponges and Cs-sponges activated at various temperatures were assessed by using N_2 gas adsorption-desorption (Figure 2). Commercial activated carbon (surface area: 1652 $m^2 g^{-1}$) was also evaluated as a reference. The Brunauer-Emmett-Teller (BET)[24] surface areas were measured to be 6, 815, 1353, 2694 $m^2 g^{-1}$ for the K-sponges, and 718, 1185, 2440, 3288 $m^2 g^{-1}$ for the Cs-sponges when activated at 400, 500, 600, and 700 °C, respectively. The main pore sizes of all the samples were below 2 nm according to the non-local density functional theory (NLDFT) method (Figure S1 in the Supporting Information)[25] verifying that both activation processes produced mainly micropores. Notably, the finding that the BET surface areas of the Cs-sponges are larger than those of the K-sponges at all the temperatures can be related to the significantly lower melting point[26] of Cs_2O (490 °C) than that of K_2O (740 °C). The BET surface areas observed for the Cs-sponges are particularly remarkable, as the value reaches 3288 $m^2 g^{-1}$ upon activation at 700 °C, in marked contrast with those of typical activated carbon of which the BET surface areas fall in the range of 1000 to 2000 $m^2 g^{-1}$. Furthermore, Cs-activation was effective even at the low temperature of 400 °C, thus more favorable for maintaining hetero-elements such as nitrogen and oxygen.

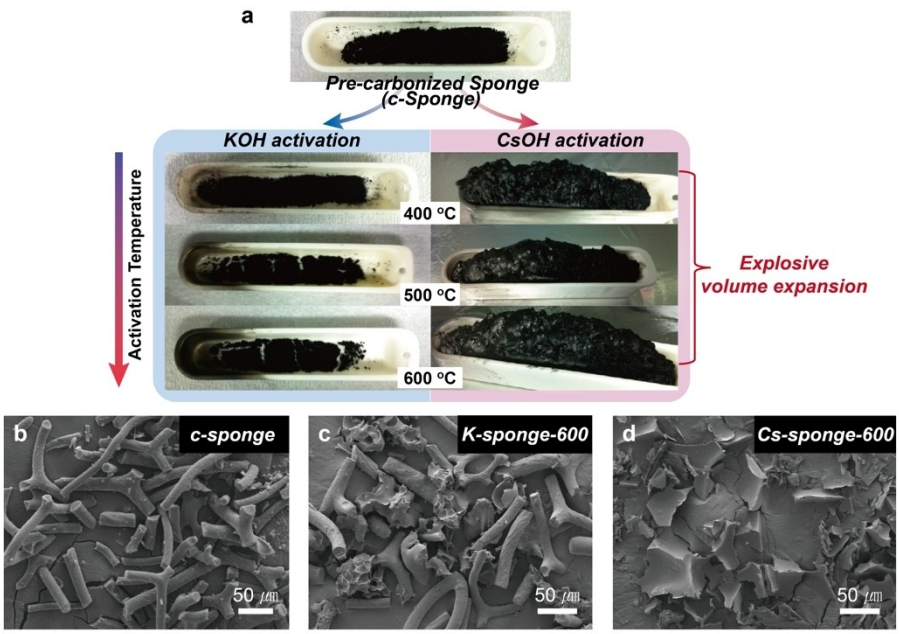

Figure 1. (a) Photographs of pre-carbonized sponge (c-sponge) and its activated forms via KOH and CsOH activation routes. Cs-sponges show explosive volume expansions compared with K-sponges. SEM images of (b) c-sponge, (c) K-sponge activated at 600 °C, and (d) Cs-sponge activated at 600 °C.

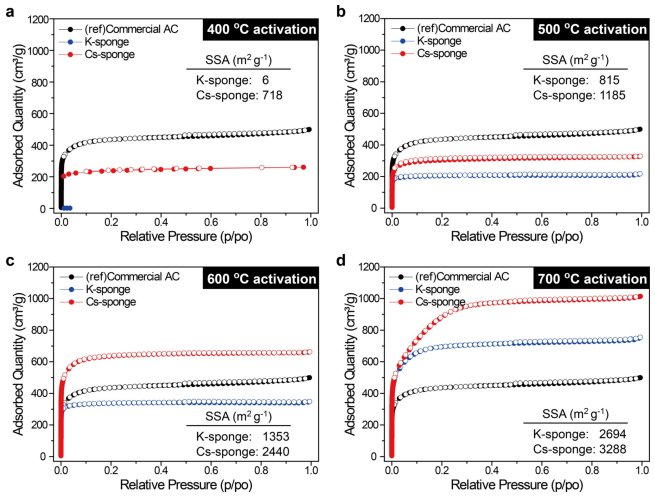

Figure 2. Comparison of N_2 adsorption-desorption curves of commercial activated carbon, K-sponges, and Cs sponges activated at different temperatures of (a) 400 °C, (b) 500 °C, (c) 600 °C, and (d) 700 °C.

The SEM and BET results prompted us to elucidate the way in which Cs-activation facilitates the activation process. In general, the activation involves both physical and chemical steps as described in the Introduction.[1,12] When the carbon host has a certain level of lattice arrangement (Figure 3), carrier ion intercalation is accompanied by the physical and chemical activation processes, and the propensity of this intercalation thus plays a critical role in relation to the lattice expansion. Because Cs-activation follows the same reaction pathway as K-activation, both of these activation processes would be expected to undergo similar physical and chemical activation. This rationale led us to suspect that the immense volume expansion during Cs-activation is associated with the facile expansion of the carbon lattice upon Cs insertion. The permeability of the carbon interlayers by an alkali metal can be correlated with the formation energy of the corresponding alkali metal-graphite intercalation compound (AM-GIC).[27–30] The formation energy of Cs-GIC is known[20,31] to be the lowest among all possible AM-GIC analogues (Li, Na, K, Rb, Cs-based), which explains the extraordinary volume expansion of the Cs-sponge despite the Cs ion having the largest radius. The same argument would be valid even for a carbon material with a moderate level of graphitization because most carbon precursors of interest to form activated carbon transform to bare carbon materials of which graphite crystallites constitute a substantial portion.[32] Thus, the preferred insertion of the Cs ion would be preserved for a majority of carbon materials regardless of the size and orientation of the graphite crystallites.

To verify the interlayer expansion during Cs-activation, transmission electron microscopy (TEM) analysis was carried out at high magnification. To this end, graphite with high crystallinity was used as a carbon source, instead of Cs-carbonized sponge, to measure the interlayer distance explicitly. Although both K- and Cs-activated graphite were observed to have undergone volume expansion, the extent of this expansion was far more pronounced for the Cs-activated graphite (Figure S2), which is consistent with the findings for the aforementioned activated sponges. The TEM image of the pristine graphite exhibits a long-range ordered layered structure with a regular interlayer distance of 3.36 Å (Figure S3). After Cs-activation, the long-range ordering of graphite was replaced by smaller areas with shorter range ordering (Figure 4a), which corresponds with the overall structural irregularity and volume expansion. In contrast, the layered structure is relatively well maintained in K-activated graphite (Figure 4b). High-resolution TEM (HRTEM) analysis indicates that the interlayer distances of

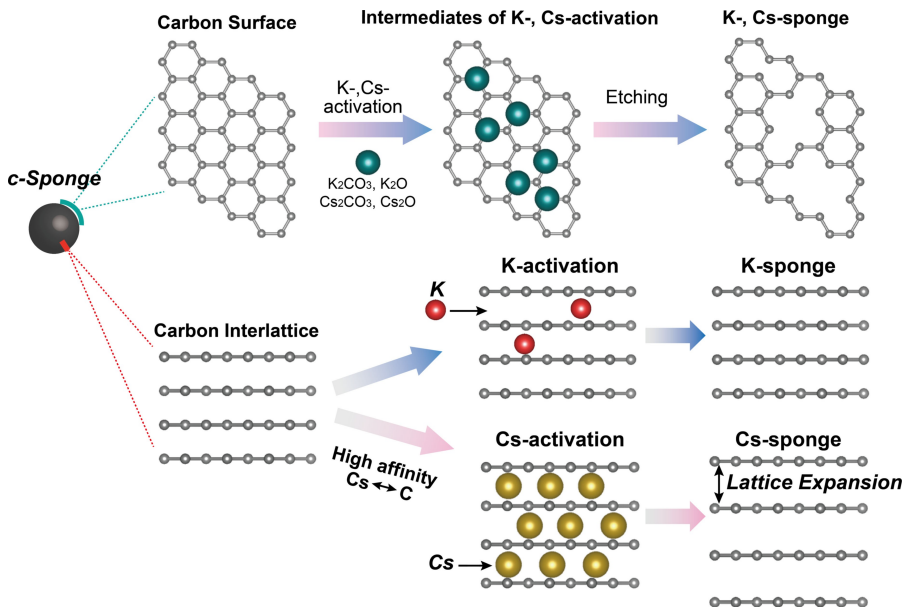

Figure 3. Suggested mechanisms of K- and Cs-activation.

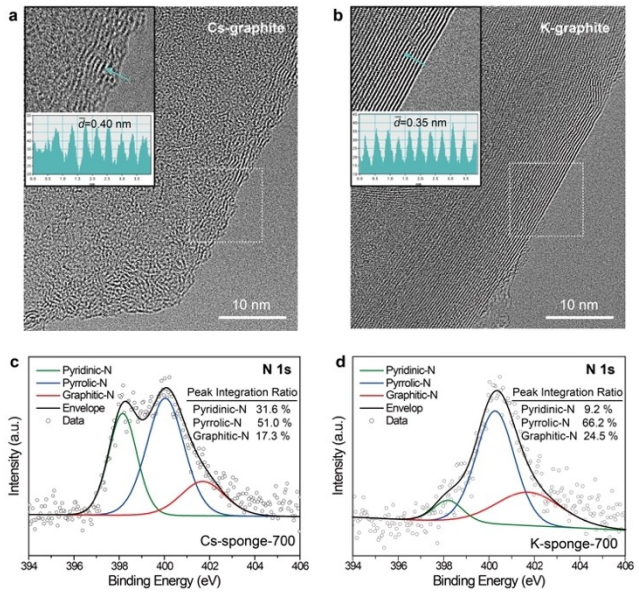

Figure 4. TEM images of (a) Cs-activated graphite and (b) K-activated graphite. (Insets) HRTEM images magnified from the areas enclosed by the white dotted boxes in the TEM images along with their line-scanning profiles. XPS N1s analysis of (c) Cs-sponge and (d) K-sponge when activated at 700 °C.

the Cs- and K-activated graphite are 0.42 and 0.37 Å, respectively, verifying lattice expansion to be the main driving force behind the structural perturbation and volume expansion of the Cs-sponge.

X-ray photoelectron spectroscopy (XPS) analysis provides information about the elemental configuration of the Cs- and K-sponges when activated at 700 °C (Figure S4). The N 1s spectra of both the Cs- and K-sponges (Figure 4c and d) exhibited three peaks at 398.2, 400.1, and 401.6 eV corresponding to the N-6 (pyridine-like), N-5 (pyrrole-like), and N–Q (graphite-like) configurations, respectively.[33–35] From these XPS data, it was noted that the Cs-sponge contains a substantial N-6 configuration of 31.6%, whereas the K-sponge contains only 9.2%. This XPS result is particularly remarkable, as pyridine-like nitrogen is well known to be unstable at high temperature compared with the other two configurations.[34,36] Pyridine-like nitrogen is characterized as a Lewis base owing to its lone-pair electrons and readily forms complexes with a metal ion.[34,37,38] On the basis of the XPS results, we thus speculate that the intercalated Cs ions are effectively bound with pyridine-like nitrogen to form metal-pyridinic nitrogen complexes, which contributes to the high portion of pyridine-like nitrogen even after the activation process at high temperature of 700 °C.

Both types of sponges were investigated as sorbents for CO_2 storage by assessing the CO_2 uptake at 273, 298, and 323 K for the sponges activated at various temperatures.[39] In addition, the commercial activated carbon with a surface area of 1652 $m^2 g^{-1}$ was measured for CO_2 and N_2 uptakes as a control (Figure S5).

All of the samples showed reversible CO_2 and N_2 isotherms at all the temperatures (Figure 5 and Figure S6), indicating physisorption-dominant uptake processes.[40,41] The physisorption uptake behavior of K-sponge and Cs-sponge are also reflected in the small values of isosteric heat of adsorption (Q_{st}). At low loadings, Q_{st} values of the K-sponge and Cs-sponge activated at 600 °C are only 26.8 and 20.8 kJ mol^{-1}, respectively (Figure S7).[42] First, it should be noted that, according to the elemental analysis, the nitrogen-to-carbon ratio of both the Cs- and K-sponges is almost the same as long as they are activated at the same temperature (Table S1). Therefore, the nitrogen content itself depends mainly on the activation temperature. In terms of the CO_2 uptake, at the same activation temperature of 400 °C, the K-sponge exhibited CO_2 uptake capacities of 114, 90, and 71 mg g^{-1} at 273, 298, and 323 K, respectively, for 1 bar (Figure 5b, d, and f). In contrast, the CO_2 uptake capacities of the Cs-sponge were much higher at 247, 170, and 118 mg g^{-1} at the same temperatures (Figure 5a, c, and e), respectively. The higher uptake capacities of the Cs-sponge are attributed to its higher surface area in spite of the low activation temperature. The effect of nitrogen on the ability to capture CO_2 was determined by comparing the Cs-sponge activated at 500 °C (referred to as Cs-sponge-500 and similarly for other samples hereafter) and K-sponge-600 because they have similar specific surface areas of 1185 and 1353, respectively. Cs-sponge-500 showed CO_2 uptake capacities of 348, 219, and 143 mg g^{-1} at 273, 298, and 323 K, respectively, whereas the corresponding values for K-sponge-600 were 190, 122, and 103 mg g^{-1} at the same temperatures. The larger uptake amounts of Cs-sponge-500 can be interpreted on the basis of its higher nitrogen content, which can induce favorable quadrupole-dipole interaction[43–47] with the N-containing units exploiting the polarizable nature of CO_2. Owing to the same advantage, remarkably, the CO_2 uptake of Cs-sponge-600 was as high as 483 mg g^{-1} at 273 K, which is conspicuously higher than that of most activated carbon materials reported to date (Table S2).[48,49] For reference, the CO_2 uptakes of the aforementioned commercial activated carbon without nitrogen contents were measured to be 212 and 122 mg g^{-1} at 273 and 298 K, respectively (Figure S5).[50–53] In summary, Cs-activation process at the relatively low temperature of 600 °C enables the high surface area of activated sponge, maintaining a high portion of nitrogen composition of the carbon substance, which is beneficial for high CO_2 uptake.

The Henry selectivities of the Cs- and K-sponges exhibited the same trend as the uptake capacity. These results are reported in Table 1, which shows that the selectivities of the Cs-sponges are consistently higher compared to those of the K-sponges at the same activation temperature, except for one case: activation at 400 °C with the uptake measured at 323 K. However, this is due to the abnormal situation in which the weak activation of the K-sponge at 400 °C results in the extremely low uptake of N_2, i.e., only 2 mg g^{-1} (Table 1).

Considering the highly efficient Cs-activation, Cs-sponge-700 and K-sponge-700 were evaluated as cathodes for lithium ion capacitors (LICs). LICs are usually coined as an intermediate electrochemical energy storage system between rechargeable batteries and supercapacitors.[54–56] Because an LIC normally adopts graphite as the anode, the specific capacity of the

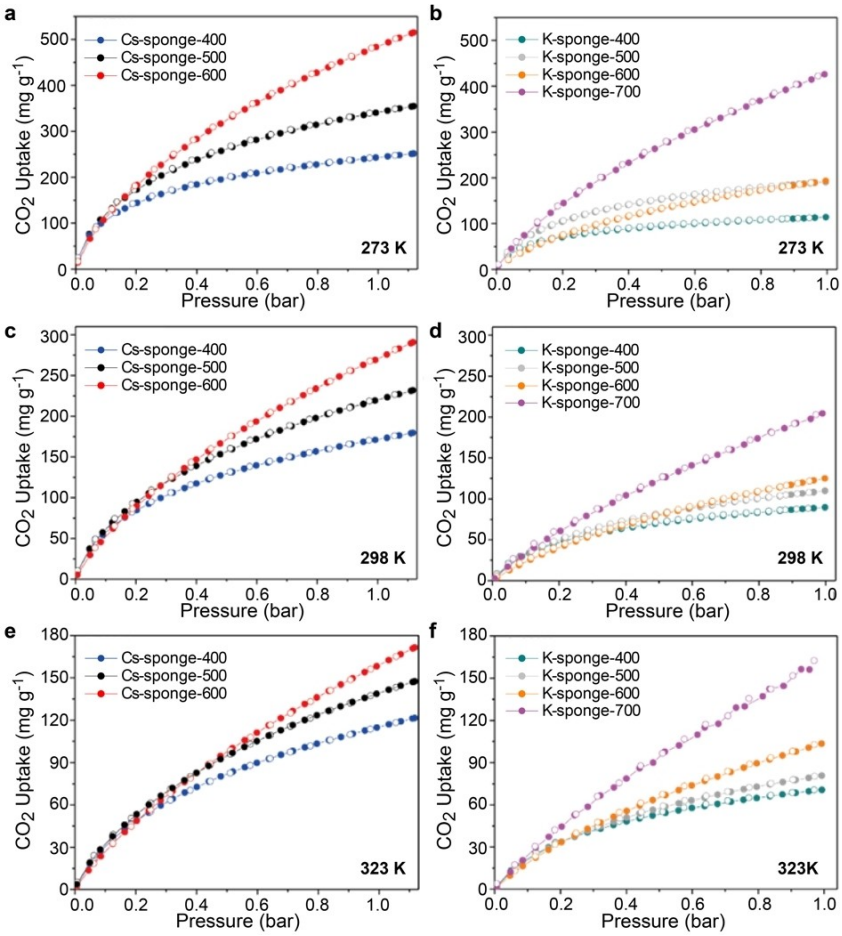

Figure 5. CO_2 uptake isotherms of Cs- and K-sponges measured at (a,b) 273 K, (c,d) 298 K, and (e,f) 323 K. The activation temperatures of each sample are represented by different color codes: 400 °C (blue), 500 °C (black), and 600 °C (red) for Cs-sponges; 400 °C (green), 500 °C (grey), 600 °C (orange), and 700 °C (magenta) for K-sponges.

Table 1. CO_2 and N_2 uptakes, CO_2/N_2 selectivities of Cs-and K-sponges activated at different temperatures.

Activation temperature [°C]		CO_2 uptake[a]			N_2 uptake[a]			Selectivity[b]		
		273 K	298 K	323 K	273 K	298 K	323 K	273 K	298 K	323 K
400	Cs-sponge	247	170	118	19	12	8	39	53	40
	K-sponge	114	90	71	6	3	2	21	34	61
500	Cs-sponge	348	219	143	22	13	8	36	40	30
	K-sponge	189	110	85	11	6	4	20	19	26
600	Cs-sponge	483	268	165	28	18	11	33	33	23
	K-sponge	190	122	103	12	6	4	13	12	22
700	K-sponge	436	212	160	18	15	10	17	9	9

[a] Unit: mg g^{-1} at 1 bar. [b] Obtained from the initial slope of the adsorption isotherm in the linear low-pressure regime (0.0–0.1 bar).

cathode plays a critical role in determining the overall energy density.[57,58] With this concern in mind, both sponges were tested as LIC cathodes by pairing them with a Li metal anode. The measurements were conducted in galvanostatic mode in the potential range of 1.5–4.5 V at a current density of 0.5 A g^{-1}. Detailed experimental conditions are provided in the Experimental Section. Commercial activated carbon (specific surface area = 1652 $m^2 g^{-1}$) was also measured as a control sample. Figure 6a displays the typical galvanostatic curves of the three electrodes during their charge and discharge processes. At the same current density of 0.5 A g^{-1}, Cs-sponge-700, K-sponge-700, and commercial activated carbon exhibited specific capacities of 115.0, 95.1, and 79.5 mAh g^{-1}, respectively. The specific capacity of Cs-sponge-700 is greater than those of most activated carbon materials tested under similar conditions, as tabulated in Table S3. The higher specific capacity of Cs-sponge-700 compared to that of K-sponge-700 is ascribed to the higher surface area and pyridinic nitrogen content of the Cs-sponge. In particular, the pyridinic nitrogen configuration is known to be beneficial for Li-ion storage because of its higher

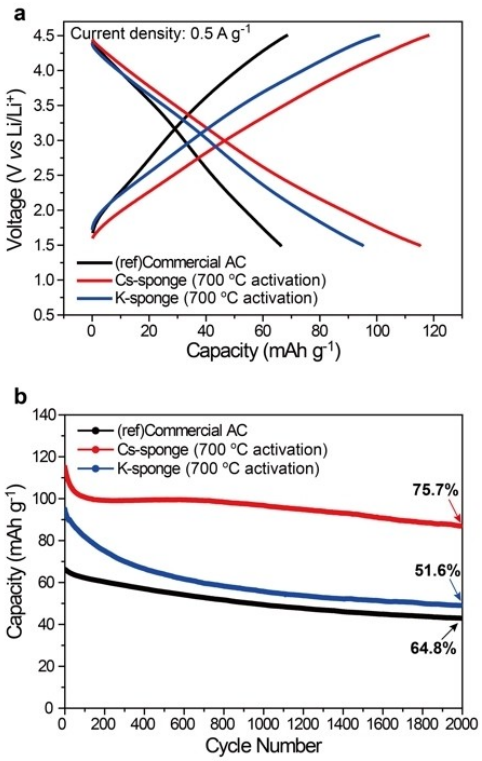

Figure 6. Electrochemical results of Cs-sponge-700 and K-sponge-700 together with that of commercial activated carbon when tested as cathodes for lithium ion capacitors. (a) Charge-discharge profiles and (b) cycle lives of Cs-sponge (red), K-sponge (blue), and commercial activated carbon (black) at a current density of 0.5 A g^{-1}.

affinity for Li ions.[59–62] Cs-sponge-700 also showed superior sustainability during cycling, considering that Cs-sponge-700, K-sponge-700, and commercial AC retained 75.7%, 51.6%, and 64.8% of their original capacities after 2000 cycles, respectively (Figure 6b). The superior cyclability of Cs-sponge-700 can also be explained by its higher content of pyridinic nitrogen, which lessens the Li^+—Li^+ repulsion near the surface such that the alignment of the Li ion flux inside the pores is enhanced, thereby inducing more uniform and robust adsorption-desorption cycles.[36,63]

Conclusion

In conclusion, we investigated the anomalously large specific surface area of activated carbon prepared *via* Cs ion mediation. The high affinity of the carbon lattice for the Cs ion facilitates lattice expansion during the activation process mediated by the Cs ions, which serves as the origin of the large surface area of Cs-sponges. Cs ion-mediated activation is effective even at temperatures as low as 400 °C. The facile complexation of the Cs ion with the pyridinic nitrogen together with the fact that low-temperature activation is possible both contribute to maintaining the nitrogen content of the sponge. In combination, the rich nitrogen content and large surface area of the resultant Cs-sponges provide a favorable environment for CO_2 capture. The Cs-sponges with their substantial pyridinic nitrogen content demonstrated superior specific capacity and cyclability for Li ion storage when tested as LIC cathodes. The findings of this study offer useful insights into the use of Cs ion-mediated activation to endow activated carbon with advantageous properties, i.e., the capability of tuning the porosity and elemental heterogeneity by exploiting the facile complexation between the intercalant ions and the carbon host during the activation process.

Experimental Section

Preparation of Cs- and K-sponges

Cs- and K-sponges were synthesized *via* the classical chemical activation process. All reagents were purchased from Sigma-Aldrich and used without any purification. Marine sponge (Mediterranean natural seal sponge-silk fine, m-sponge) was purchased from Spugnificio Bellini Egidio Di Bellini Ivano E C. Snc, Italy. Pre-carbonized sponge (*c*-sponge) was obtained by sintering m-sponge at 300 °C for 4 h. Then, 0.4 g of *c*-sponge and 0.01 mol of cesium hydroxide monohydrate ($CsOH{\cdot}H_2O$, 99.95%) were dispersed in 20 mL of deionized water and vigorously stirred at 60 °C. After evaporating the water, the mixed precursors were dried at 100 °C overnight. The dried sample was sintered at 120 °C for 1 h to remove adsorbed water and further sintered at the respective target activation temperature (400, 500, 600, and 700 °C) for 1 h to produce the Cs-sponges. The entire activation process was conducted under Ar flow (300 sccm). To avoid potential danger of pyrophoricity, all of the final samples were cooled down to room temperature under the Ar atmosphere. The obtained Cs-sponges were thoroughly washed with hydrochloric acid (35 wt%, 100 mL) to remove any inorganic residues, and subsequently several times with deionized water (2000 mL) and ethanol until the pH reached 7. Finally, the produced Cs-sponges were dried inside an oven at 70 °C for 24 h. The K-sponges were prepared by using the same process except that potassium hydroxide (KOH, $\geq$99.95%) was used as an activation agent. The commercial activated carbon (YP-50F) was purchased from Kuraray. Samples of Cs- and K-graphite were also activated using the aforementioned procedure at the activation temperature of 700 °C. The precursor for the activated graphite was purchased from Sigma-Aldrich (Graphite, synthetic).

Characterization

Field emission-scanning electron microscopy (FE-SEM, JSM-6700F, JEOL Ltd, Japan) was employed to observe the morphologies of the *c*-sponge, Cs-sponge, and K-sponge samples. To evaluate the porosity of the Cs- and K-sponges, N_2 adsorption-desorption isotherms were recorded by using a porosity analyzer (Micromeritics 3Flex, USA) operating at 77 K. Commercial activated carbon (YP50F, Kuraray, Japan) was measured as a reference. Prior to the porosity measurement, each sample was degassed at 120 °C for 12 h. The specific surface area was calculated based on the Brunauer-Emmett-Teller (BET) method. Pore size distribution was obtained by the non-local density functional theory (NLDFT) method assuming slit-shaped pore geometry. Isosteric heat of adsorption(Q_{st}) values were obtained from adsorption data using the Clausius-Clapeyron equation. Field emission-transmission electron microscopy (FE-TEM, JEM-F200, JEOL Ltd, Japan) was used to visualize the morphologies of the activated graphite samples at an acceleration voltage of 200 kV. X-ray photoelectron spectroscopy

(XPS, K-alpha, Thermo VG Scientific) analysis and elemental analysis (FlashSmart, Thermo Fisher Scientific) were performed to obtain the elemental information. The CO_2 and N_2 adsorption-desorption isotherms were attained at 273, 298, and 323 K in the pressure range of 0–1 bar by using the porosity analyzer (Micromeritics 3Flex, USA). During the measurements, the temperature was kept constant by using an iso-temperature controller (ProtechKorea, Korea).

Electrochemical Measurement

The Cs-sponge, K-sponge, and commercial activated carbon electrodes were fabricated by first dispersing the active material, super-P (TIMCAL), and poly(vinylidene difluoride) (PVDF, Sigma-Aldrich) in *N*-1-methyl-2-pyrrolidine (NMP, Sigma-Aldrich) at a mass ratio of 8:1:1. The slurries were then cast onto aluminum foil. The mass loadings of the active materials were 1.5–1.7 mg cm^{-2}. The electrolyte solution contained 1 M lithium hexafluorophosphate ($LiPF_6$) dissolved in co-solvents of ethylene carbonate (EC) and dimethyl carbonate (DMC) (50:50 = *v*:*v*). The 2032-type coin cells were fabricated in an Ar-filled glovebox using a polypropylene membrane (2400, Celgard) as separator. Electrochemical tests of the Cs-sponge, K-sponge, and commercial AC were conducted in the potential range of 1.5–4.5 V (*vs.* Li/Li$^+$) at a current density of 0.5 A g^{-1} using a battery cycler (WBCS3000 L, Wonatech) at 25 °C. Experimental Details.

Acknowledgements

We acknowledge financial support from a National Research Foundation of Korea grant (NRF-2017M1A2A2044504, NRF-2018R1A2A1A19023146, and NRF-2018M1A2A2063340) and generous support from Institute of Inter-university Semiconductor Research Center (ISRC) Engineering Research (IER) at Seoul National University.

Conflict of Interest

The authors declare no conflict of interest.

Keywords: activated carbon · graphite intercalation compounds · CO_2 capture · Li-ion storage

[1] H. Marsh, F. R. Reinoso, *Activated carbon*, Elsevier **2006**.
[2] L. L. Zhang, X. Zhao, *Chem. Soc. Rev.* **2009**, *38*, 2520–2531.
[3] A. L. Chaffee, G. P. Knowles, Z. Liang, J. Zhang, P. Xiao, P. A. Webley, *Int. J. Greenhouse Gas Control* **2007**, *1*, 11–18.
[4] Y. Zhu, S. Murali, M. D. Stoller, K. Ganesh, W. Cai, P. J. Ferreira, A. Pirkle, R. M. Wallace, K. A. Cychosz, M. Thommes, *Science* **2011**, *332*, 1537–1541.
[5] A. S. Jalilov, G. Ruan, C.-C. Hwang, D. E. Schipper, J. J. Tour, Y. Li, H. Fei, E. L. Samuel, J. M. Tour, *ACS Appl. Mater. Interfaces* **2015**, *7*, 1376–1382.
[6] P. Simon, Y. Gogotsi, *Nanoscience and technology: a collection of reviews from Nature journals*, World Scientific **2010**; pp 320–329.
[7] A. Samanta, A. Zhao, G. K. Shimizu, P. Sarkar, R. Gupta, *Ind. Eng. Chem. Res.* **2012**, *51*, 1438–1463.
[8] M. Lillo-Ródenas, D. Cazorla-Amorós, A. Linares-Solano, *Carbon* **2003**, *41*, 267–275.
[9] J. H. Lee, K. Kwac, H. J. Lee, S. Y. Lim, D. S. Jung, Y. Jung, J. W. Choi, *ChemNanoMat* **2016**, *2*, 528–533.
[10] J. Romanos, M. Beckner, T. Rash, L. Firlej, B. Kuchta, P. Yu, G. Suppes, C. Wexler, P. Pfeifer, *Nanotechnology* **2011**, *23*, 015401.
[11] T. Otowa, R. Tanibata, M. Itoh, *Gas Sep. Purif.* **1993**, *7*, 241–245.
[12] J. Wang, S. Kaskel, *J. Mater. Chem.* **2012**, *22*, 23710–23725.
[13] E. Raymundo-Pinero, P. Azaïs, T. Cacciaguerra, D. Cazorla-Amorós, A. Linares-Solano, F. Béguin, *Carbon* **2005**, *43*, 786–795.
[14] R. L. Zornitta, K. M. Barcelos, F. G. Nogueira, L. A. Ruotolo, *Carbon* **2020**, *156*, 346–358.
[15] W. Wang, S. Xu, K. Wang, J. Liang, W. J. F. P. T. Zhang, *Fuel Process. Technol.* **2019**, *189*, 74–79.
[16] C. Pevida, M. G. Plaza, B. Arias, J. Fermoso, F. Rubiera, J. Pis, *Appl. Surf. Sci.* **2008**, *254*, 7165–7172.
[17] H. M. Jeong, J. W. Lee, W. H. Shin, Y. J. Choi, H. J. Shin, J. K. Kang, J. W. Choi, *Nano Lett.* **2011**, *11*, 2472–2477.
[18] N. P. Wickramaratne, J. Xu, M. Wang, L. Zhu, L. Dai, M. Jaroniec, *Chem. Mater.* **2014**, *26*, 2820–2828.
[19] J. Wei, D. Zhou, Z. Sun, Y. Deng, Y. Xia, D. Zhao, *Adv. Funct. Mater.* **2013**, *23*, 2322–2328.
[20] Y. Liu, B. V. Merinov, W. A. Goddard, *Proc. Mont. Acad. Sci.* **2016**, *113*, 3735–3739.
[21] H. Moriwake, A. Kuwabara, C. A. Fisher, Y. Ikuhara, *RSC Adv.* **2017**, *7*, 36550–36554.
[22] M. Lillo-Ródenas, J. Juan-Juan, D. Cazorla-Amorós, A. Linares-Solano, *Carbon* **2004**, *42*, 1371–1375.
[23] S. Mitani, S.-I. Lee, S.-H. Yoon, Y. Korai, I. Mochida, *J. Power Sources* **2004**, *133*, 298–301.
[24] S. Brunauer, P. H. Emmett, E. Teller, *J. Am. Chem. Soc.* **1938**, *60*, 309–319.
[25] C. Lastoskie, K. E. Gubbins, N. Quirke, *Langmuir* **1993**, *9*, 2693–2702.
[26] P. Touzain, *J. Therm. Anal.* **1976**, *9*, 441–450.
[27] Y. Li, Y. Lu, P. Adelhelm, M.-M. Titirici, Y.-S. Hu, *Chem. Soc. Rev.* **2019**, *48*, 4655–4687.
[28] K. Nobuhara, H. Nakayama, M. Nose, S. Nakanishi, H. Iba, *J. Power Sources* **2013**, *243*, 585–587.
[29] W.-B. Li, S.-Y. Lin, N. T. T. Tran, M.-F. Lin, K.-I. Lin, *RSC Adv.* **2020**, *10*, 23573–23581.
[30] J.-X. Huang, G. Csányi, J.-B. Zhao, J. Cheng, V. L. Deringer, *J. Mater. Chem. A* **2019**, *7*, 19070–19080.
[31] G. Yoon, H. Kim, I. Park, K. Kang, *Adv. Energy Mater.* **2017**, *7*, 1601519.
[32] K. Dasgupta, D. Sathiyamoorthy, *Mater. Sci. Technol.* **2003**, *19*, 995–1002.
[33] F. Kapteijn, J. Moulijn, S. Matzner, H.-P. Boehm, *Carbon* **1999**, *37*, 1143–1150.
[34] Y. Mao, H. Duan, B. Xu, L. Zhang, Y. Hu, C. Zhao, Z. Wang, L. Chen, Y. Yang, *Energy Environ. Sci.* **2012**, *5*, 7950–7955.
[35] R. Jansen, H. Van Bekkum, *Carbon* **1995**, *33*, 1021–1027.
[36] Y. Li, Z. Zhou, L. Wang, *J. Chem. Phys.* **2008**, *129*, 104703.
[37] Y.-C. Lin, P.-Y. Teng, C.-H. Yeh, M. Koshino, P.-W. Chiu, K. Suenaga, *Nano Lett.* **2015**, *15*, 7408–7413.
[38] S. Pal, *Pyridine: A useful ligand in transition metal complexes*, IntechOpen **2018**.
[39] C. Lu, H. Bai, B. Wu, F. Su, J. F. Hwang, *Energy Fuels* **2008**, *22*, 3050–3056.
[40] V. Chandra, S. U. Yu, S. H. Kim, Y. S. Yoon, D. Y. Kim, A. H. Kwon, M. Meyyappan, K. S. Kim, *Chem. Commun.* **2012**, *48*, 735–737.
[41] M. Nandi, K. Okada, A. Dutta, A. Bhaumik, J. Maruyama, D. Derks, H. Uyama, *Chem. Commun.* **2012**, *48*, 10283–10285.
[42] Z. Wu, P. A. Webley, D. Zhao, *J. Mater. Chem.* **2012**, *22*, 11379–11389.
[43] J. H. Lee, H. J. Lee, S. Y. Lim, B. G. Kim, J. W. Choi, *J. Am. Chem. Soc.* **2015**, *137*, 7210–7216.
[44] P. Z. Li, Y. Zhao, *Chem. Asian J.* **2013**, *8*, 1680–1691.
[45] D. M. D'Alessandro, B. Smit, J. R. Long, *Angew. Chem. Int. Ed.* **2010**, *49*, 6058–6082; *Angew. Chem.* **2010**, *122*, 6194–6219.
[46] H. A. Patel, S. H. Je, J. Park, D. P. Chen, Y. Jung, C. T. Yavuz, A. Coskun, *Nat. Commun.* **2013**, *4*, 1–8.
[47] E. Qezelsefloo, S. Khalili, M. Jahanshahi, M. Peyravi, *Mater. Chem. Phys.* **2020**, *239*, 122304.
[48] A. Samanta, A. Zhao, G. K. Shimizu, P. Sarkar, R. Gupta, *Ind. Eng. Chem. Res.* **2012**, *51*, 1438–1463.
[49] J. Wang, L. Huang, R. Yang, Z. Zhang, J. Wu, Y. Gao, Q. Wang, D. O'Hare, Z. Zhong, *Energy Environ. Sci.* **2014**, *7*, 3478–3518.
[50] C. Zhang, W. Song, Q. Ma, L. Xie, X. Zhang, H. Guo, *Energy Fuels* **2016**, *30*, 4181–4190.
[51] M. Sevilla, A. B. Fuertes, *Energy Environ. Sci.* **2011**, *4*, 1765–1771.
[52] M. Sevilla, A. S. M. Al-Jumialy, A. B. Fuertes, R. Mokaya, *ACS Appl. Mater. Interfaces* **2018**, *10*, 1623–1633.
[53] G. Singh, K. S. Lakhi, K. Ramadass, C. Sathish, A. Vinu, *ACS Sustainable Chem. Eng.* **2019**, *7*, 7412–7420.

[54] Y. Ma, H. Chang, M. Zhang, Y. Chen, *Adv. Mater.* **2015**, *27*, 5296–5308.
[55] V. Aravindan, J. Gnanaraj, Y.-S. Lee, S. Madhavi, *Chem. Rev.* **2014**, *114*, 11619–11635.
[56] G. G. Amatucci, F. Badway, A. Du Pasquier, T. Zheng, *J. Electrochem. Soc.* **2001**, *148*, A930–A939.
[57] S. R. Sivakkumar, A. Pandolfo, *Electrochim. Acta* **2012**, *65*, 280–287.
[58] H. Wang, Y. Zhang, H. Ang, Y. Zhang, H. T. Tan, Y. Zhang, Y. Guo, J. B. Franklin, X. L. Wu, M. Srinivasan, *Adv. Funct. Mater.* **2016**, *26*, 3082–3093.
[59] L. Bulusheva, E. Fedorovskaya, A. Kurenya, A. Okotrub, *Phys. Status Solidi B* **2013**, *250*, 2586–2591.
[60] C. Zhan, Y. Zhang, P. T. Cummings, D.-e. Jiang, *Phys. Chem. Chem. Phys.* **2016**, *18*, 4668–4674.
[61] G. Luo, L. Liu, J. Zhang, G. Li, B. Wang, J. Zhao, *ACS Appl. Mater. Interfaces* **2013**, *5*, 11184–11193.
[62] J. H. Lee, N. Park, B. G. Kim, D. S. Jung, K. Im, J. Hur, J. W. Choi, *ACS Nano* **2013**, *7*, 9366–9374.
[63] A. L. M. Reddy, A. Srivastava, S. R. Gowda, H. Gullapalli, M. Dubey, P. M. Ajayan, *ACS Nano* **2010**, *4*, 6337–6342.

Manuscript received: October 8, 2020
Revised manuscript received: November 28, 2020
Accepted manuscript online: November 30, 2020
Version of record online: December 16, 2020